Joint Power Waveforming and Beamforming for Wireless Power Transfer

Meng-Lin Ku, *Member, IEEE*, Yi Han, Beibei Wang, *Senior Member, IEEE*, and K. J. Ray Liu, *Fellow, IEEE*

***Abstract*—In the Internet of Things, wireless devices need more easily accessible energy resources, which motivates the development of wireless power transfer (WPT) using radio frequency signals. Beamforming technique has been widely adopted by using multiple transmit antennas to form a sharp energy beam toward an intended receiver. However, few of them have considered the potential gain of multipath propagation. In this paper, we propose a joint power waveforming and beamforming in the time domain for WPT, in which the waveforms on multiple transmit antennas driven by a common reference signal are designed to maximize the gain of energy delivery efficiency. We consider both nonperiodic and periodic reference signals and propose low-complexity waveforms that can achieve near-optimal performance. It is found that the energy delivery efficiency gain of the proposed approach increases with the waveform length until saturation. We theoretically analyze the outage probability of the proposed approach under a uniform power delay channel profile, which quantifies the impact of the number of antennas and multipaths. Simulations are performed to validate the theoretic analysis and the effectiveness of the proposed joint power waveforming and beamforming approach.**

***Index Terms*—Wireless power transfer, power waveforming, multiple antennas, ultra-wideband, multipath channels.**

I. Introduction

In THE era of Internet of Things (IoT), it is anticipated that low-power wireless devices, e.g., home appliances, security sensors, smart meters, are widely deployed as fundamental building blocks to support numerous wireless data applications [1], [2]. These wireless devices are often untethered to a power grid and merely rely on equipped batteries for the operation over a long period of time. In addition to the availability of spectrum resources, which is a common issue for the conventional wireless networks, wireless devices in the future are thus constrained by the limited battery capacity due to massive wireless data services. For IoT applications, wireless devices are sometimes eager for more energy resources, rather than spectrum resources, since low-rate data may be continuously and perpetually reported from devices to devices. Besides, the deployment of nodes in poisonous and even unreachable environments does not allow for frequent battery replacement when the battery is exhausted. In recent years, energy harvesting techniques, by which wireless devices are able to harvest and store energy by using rechargeable batteries, have been emerged as an effective way for avoiding the cost and the challenge of battery replacement [3].

In general, energy harvesting nodes can scavenge energy from either ambient energy sources, e.g., solar, wind, and vibration, or dedicated energy sources, e.g., power stations, to prolong the network lifetime [4]. While ambient energy sources are environmentally-friendly, the main drawback of these energy sources lies in that the uncertain nature in time, location and weather conditions makes it difficult to guarantee the quality-of-services (QoS) of wireless communications. On the other hand, dedicated energy emitted by power stations are attractive alternatives to supply on-demand energy for wirelessly replenishing devices and fully controllable to meet the QoS requirements even though an additional cost is incurred with the deployment of power stations, in comparison with the ambient energy sources [5]. The rapid proliferation of energy harvesting communications has urged the development of wireless power transfer (WPT) using electromagnetic radiation, which has been recognized as a promising solution to sustain energy for rechargeable low-power wireless devices over the air. Electromagnetic induction coupling, magnetic resonant coupling, and radio frequency (RF) signals are three common WPT approaches [6]. As compared with the former two approaches which only afford a limited working range of a few centimeters, the adoption of a RF signal as a medium is capable of wirelessly charging nodes over a long distance (up to several meters) [7]. Considering its potential in far-end WPT applications, we will concentrate on the investigation of RF signal-based WPT systems in this paper.

A major concern for designing the RF signal-based power transfer systems is the low power transfer efficiency due to the severe radio wave propagation loss, including multipath, shadowing and large-scale path loss over distance. According to the law of energy conservation, only a small portion of energy radiated from a transmitter can be harvested at a receiver in reality, yielding an energy scarcity problem. Moreover, unlike the conventional information receivers, energy receivers require much higher receiver sensitivity to convert RF signals into DC power via rectifier circuits, which makes the design even more

Manuscript received April 19, 2017; revised August 5, 2017; accepted September 1, 2017. Date of publication September 21, 2017; date of current version October 20, 2017. The associate editor coordinating the review of this manuscript and approving it for publication was Prof. Rui Zhang. *(Corresponding author: Beibei Wang.)*

M.-L. Ku is with the Origin Wireless, Inc., Greenbelt, MD 20770 USA, and also with the Department of Communication Engineering, National Central University, Taoyuan City 32001, Taiwan (e-mail: mlku@ce.ncu.edu.tw).

Y. Han, B. Wang, and K. J. Ray Liu are with the Origin Wireless, Inc., Greenbelt, MD 20770 USA, and also with the Department of Electrical and Computer Engineering, University of Maryland, College Park, MD 20742 USA (e-mail: yhan1990@umd.edu; bebewang@umd.edu; kjrliu@umd.edu).

Color versions of one or more of the figures in this paper are available online at http://ieeexplore.ieee.org.

Digital Object Identifier 10.1109/TSP.2017.2755582

challenging, e.g., -50 dBm for information receivers and -10 dBm for energy receivers [8].

To overcome the aforementioned problem, beamforming techniques have been widely adopted to achieve efficient power transfer by synthesizing a sharp energy beam toward an intended receiver through multiple transmit antennas. Since the transmitter is capable of concentrating the radiated energy toward a particular direction, the power intensity is significantly magnified in the direction of the intended receiver. Various research efforts have been made to improve the WPT performance along this line [9]–[24]. The performance enhancement with multi-antenna configurations was investigated in [9], and a performance tradeoff between wireless information and power transfer was theoretically analyzed. The authors in [10] compared isotropic and directional beamforming antennas in randomly deployed power stations, based on a stochastic geometry model, for charging mobile terminals wirelessly. In [11], energy beamforming was designed for powering RF identification (RFID) tags. In [12], an adaptive WPT scheme was considered for a large scale sensor network by adapting energy beams to charge the nearby sensors, and stochastic geometry was utilized to derive the distribution of aggregated received power and the active probability of sensors. Massive antennas were applied in [13] and [14] for WPT, and the effect of the number of antennas on the performance was comprehensively analyzed. Moreover, the probability of outage in wireless energy transfer was analyzed in [15] for a base station using massive antenna arrays over flat fading channels. The authors in [16] studied energy beamforming in wireless-powered cellular networks, where downlink energy was used to sustain users during the uplink transmission. The work [17] extended [16] by deriving the asymptotically optimal power allocation for energy beamforming. For broadband wireless systems with multiple transmit antennas, the wideband channel is partitioned into several frequency sub-bands, and the signals on the sub-bands are optimized in the frequency domain to maximize the harvested power at the receiver in [18]–[23]. An overview on multi-band WPT that exploits both beamforming and frequency diversity gains was provided in [20], while a power control problem was cast in [21] for realizing simultaneous information and power transfer in the downlink. The cost of channel training for narrow-band WPT was concerned in [22]–[24]. The authors in [22] studied channel training methods for distributed energy beamforming. In [23], beamforming, along with the time and energy costs for reverse-link channel training, was designed by exploiting the channel reciprocity. In [24], the preamble length and power allocation for channel estimation were optimized for energy beamforming.

More recently, power waveforming (PW) techniques have been first proposed in [27] to improve the WPT efficiency by exploiting multipath signals. Considering the fact that the radiated power is dispersed into multiple replicas of transmitted signals by the obstacles in wireless environments, waveforms were designed in [27] for the PW systems to constructively recollect the power of all possibly available multipaths at an energy receiver. However, the scheme only considers a single-antenna PW system and subject to the case when the number of multipaths is equal to the waveform length. In this work, we attempt to develop a joint power waveforming and beamforming design for WPT, in which the waveforms on multiple transmit antennas, driven by a reference signal, are proposed to maximize an energy delivery efficiency gain, which is defined as a ratio of the harvested energy at the receiver and the energy expenditure at the transmitter.

Most of the existing works studied the multi-antenna WPT by means of beamforming techniques over frequency flat fading channels or narrow-band transmissions [9]–[17], [22]–[26]. Based on orthogonal frequency division multiplexing (OFDM), some recent works such as [18], [21] and [28] investigated broadband WPT systems over frequency selective fading channels. However, the work [28] only addressed the problem with a single transmit antenna. For multi-antenna OFDM-based WPT systems, the work [21] focused on a joint power and sub-band allocation problem and bypassed beamforming designs, while the work [18] maximized the net harvested energy. In these two works, the sub-bands were assumed to be independent of each other, and no attempts have been made to appropriately utilize the multipath effect of wireless channels.

To the best of our knowledge, joint power waveforming and beamforming for WPT is first proposed in this paper to reap both the antenna and multipath gains in wireless channels, which is different from the narrow-band transmission. While OFDM could be one possible solution for WPT, the proposed system in this paper can be deemed as a *time-domain* waveform design approach, in which the total wideband channel is considered as a whole in the design of the time-domain reference signals and waveforms without relying on the assumption of the orthogonality of sub-bands such as in [18]–[23].[§] The main contributions of this paper are summarized as follows:

- This work is the first attempt to formulate the WPT problem by combining power waveforming and beamforming and jointly optimize the reference signal and the waveforms to maximize the energy delivery efficiency gain. Two kinds of reference signals are considered in our study: non-periodic and periodic.
- For the non-periodic transmission of the reference signals, the problem is iteratively solved by alternating between the optimization of the reference signal and the waveforms, and eigenvalue decomposition is performed at each iteration run. Based on some observations, a simple rule of thumb is found to initialize the reference signal, achieving a better performance than a randomly initialized reference signal. It is shown by simulation results that compared to conventional WPT using beamforming scheme, the proposed approach has a 20–30dB improvement in energy delivery efficiency.
- In the case of the periodic reference signals, a rigorous analysis for the structure of the optimal waveforms is conducted for the proposed multi-antenna PW systems, and several quantitative findings are provided. In this case, low-complexity single-tone waveforms, which merely concentrate the entire waveform power on a single frequency

[§]The CIR is explicitly utilized in the time-domain design, which is capable of constructively accumulating all the possibly available multipath power at the receiver in both spatial and temporal domains. The phenomenon in the temporal domain is the so-called multipath gains.

component, are proven to be the optimal choice when the waveform length is a multiple of the period of a given reference signal. The optimal power allocation and tone selection are also discussed. With the optimal waveforms, we further show that the energy delivery efficiency gain can be linearly increased by prolonging the waveform length when the noise power is sufficiently small.

- In addition, when the period of the reference signal is larger than or equal to the length of multipath channels, we prove that the optimal reference signal with periodic transmission is a complex sinusoidal signal which is determined by selecting a frequency component with the largest sum-power of channel frequency responses over multiple transmit antennas.
- With the optimal reference signal and waveform designs, we theoretically analyze the outage probability of the average harvested energy as well as the average energy delivery efficiency gain under a uniform power delay (UPD) channel profile. Specifically, an upper bound for the outage performance and a lower bound for the delivery efficiency are obtained in closed forms, which helps us to quantify the impact of the numbers of multipaths and antennas on the WPT performance. Finally, extensive computer simulations are carried out to validate the theoretical results and to demonstrate the effectiveness of the proposed multi-antenna PW schemes in various channel models.

The following notations are adopted throughout this paper. The uppercase and lowercase boldface letters denote matrices and vectors, respectively. The notations $(\cdot)^T$, $(\cdot)^\dagger$, $(\cdot)^*$, $((\cdot))_N$ and $\star$ stand for transpose, conjugate transpose, element-wise conjugate, modulo-N and convolution operation, respectively. The matrices $\mathbf{I}_N$ and $\mathbf{F}_N$ represent an $N \times N$ identity matrix and an N-point discrete Fourier transform (DFT) matrix, respectively, and the (k, n)th entry of the DFT matrix is given by $\frac{1}{\sqrt{N}} e^{-j\frac{2\pi kn}{N}}$. The notations $\mathbf{1}_N$, $\mathbf{0}_N$ and $\mathbf{e}_k$ are used to express an all-one vector, an all-zero vector, and the kth column of the identity matrix $\mathbf{I}_N$, respectively. The Kronecker product and Hadamard product are denoted by $\otimes$ and $\odot$, respectively. The notation $\mathbb{E}[\cdot]$ takes expectation, while $\|\mathbf{x}\|_2$ finds the Euclidean norm of a vector $\mathbf{x}$. The matrix $Diag[\mathbf{x}]$ represents a diagonal matrix with $\mathbf{x}$ as its diagonal entries. The operators $\boldsymbol{\zeta}_1[\mathbf{A}]$ and $\lambda_{\max}[\mathbf{A}]$ take the principal eigenvector and eigenvalue of the matrix $\mathbf{A}$, respectively.

The rest of this paper is organized as follows. In Section II, we introduce the system model for the proposed multi-antenna PW system in multipath channels. The waveform designs for non-periodic and periodic transmissions of reference signals, along with the optimization of reference signals, are presented Section III. Section IV is devoted to analyze the performance of the multi-antenna PW system, including the outage probability of the average harvested energy and the average energy delivery efficiency gain. Section V presents simulation and numerical results. Conclusions are finally drawn in Section VI.

II. System Model

The proposed multi-antenna PW system is illustrated in Fig. 1, where the transmitter is equipped with M antennas and the receiver has a single antenna. We assume that the wireless channel between each transmit and receive antenna is composed of L taps and quasi-static during the observation time. The channel impulse response (CIR) between the mth transmit antenna and the receiver is modeled as

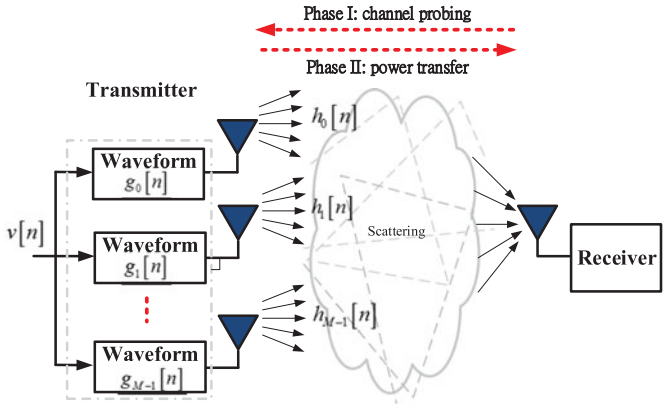

Fig. 1. The proposed multi-antenna PW system with two transmission phases: channel probing and power transfer.

$$h_m[n] = \sum_{l=0}^{L-1} h_{m,l}\,\delta[n-l], \quad n = 0, \ldots, L-1, \qquad (1)$$

where $\delta[n]$ is the Kronecker delta function, and $h_{m,l}$'s are identically and independently distributed (i.i.d.) complex Gaussian with zero mean and variance $\rho_{m,l}$, for $l = 0, \ldots, L-1$. Without loss of generality, the total channel power of each channel link is normalized to one, i.e., $\sum_{l=0}^{L-1} \rho_{m,l} = 1$, for $m = 0, \ldots, M-1$.

In Fig. 1, the implementation of the proposed multi-antenna PW system consists of two transmission phases: channel probing phase and power transfer phase. During the first phase, the receiver first sends a pilot sounding signal with a delta-like autocorrelation function to each transmit antenna for estimating the corresponding CIR [29]. The CIR can be estimated very accurately through Golay sequences and the correlation method in [30]. In practice, the number of digitally resolvable multipaths in (1), which naturally exist in the wireless environments, at the transmitter increases as the system bandwidth becomes wider, and the number of resolvable multipaths will reach an upper limit when the system bandwidth is sufficiently large [31]. With the channel reciprocity and quasi-static assumptions, the transmitter computes a waveform $g_m[n]$ for each transmit antenna based on the estimated CIR during the second phase for the WPT purpose, for $m = 0, \ldots, M-1$ and $n = 0, \ldots, N_g - 1$, and N_g is the length of the waveform. Let $v[n]$ be a reference signal of length N_v, for $n = 0, \ldots, N_v - 1$, which acts as the energy-bearing signal for continuously supplying energy. The multipath channels will disperse the radiated power to multiple replicas of the transmitted signals, resulting in the so-called inter-symbol interference (ISI) effect which causes not only the magnitude and phase variation but also the delay spread of the transmitted signals. By leveraging this effect, the waveforms are designed to constructively accumulate all the possibly available multipath power at the receiver. Hence, the reference signal after the waveform embedding at the mth transmit antenna can be

formulated as[‡]

$$s_m[n] = \sqrt{P_v}\,(v \star g_m)[n], \quad n = 0, \ldots, N_g + N_v - 2, \quad (2)$$

where we assume that the total waveform power is equal to one, i.e., $\sum_{m=0}^{M-1}\sum_{n=0}^{N_g-1}|g_m[n]|^2 = 1$, the average reference signal power is given by $\frac{1}{N_v}\sum_{n=0}^{N_v-1}|v[n]|^2 = 1$, and P_v is the average transmit power. Accordingly, the received signal at the receiver side is given as

$$\begin{aligned} y[n] &= \sum\nolimits_{m=0}^{M-1}(s_m \star h_m)[n] + z[n] \\ &= \sqrt{P_v}\sum\nolimits_{m=0}^{M-1}(v \star g_m \star h_m)[n] + z[n], \\ & n = 0, \ldots, N_g + N_v + L - 3, \end{aligned} \quad (3)$$

where $z[n]$ is additive complex white Gaussian noise at the receiver side with zero mean and variance σ_z^2.

III. Power Transfer Waveform and Reference Signal Designs

In this section, we attempt to design the reference signal as well as the waveform at each transmit antenna for the proposed multi-antenna PW system in order to maximize the energy delivery efficiency gain. While we only focus on a block transmission of $v[n]$ with the time duration of N_v in (3), the aforementioned WPT procedures can be repeated continuously with the different or the same reference signals, i.e., $v[n]$ could be non-periodic or periodic. The optimal designs of these two scenarios are investigated in the following.

Definition 1: An energy delivery efficiency gain is defined as a ratio of the total harvested energy at the receiver and the total energy expenditure of the reference signal at the transmitter.[‖]

A. Waveform Design With Non-Periodic Reference Signals

Let us first define $\mathbf{y} = [y[0], \ldots, y[N_g + N_v + L - 3]]^T$, $\mathbf{v} = [v[0], \ldots, v[N_v - 1]]^T$ and $\mathbf{h}_m = [h_m[0], \ldots, h_m[L-1]]^T$. By rewriting (3) into a compact matrix-vector form, it gives

$$\mathbf{y} = \sqrt{P_v}\sum_{m=0}^{M-1}\mathbf{V}\mathbf{H}_m\mathbf{g}_m + \mathbf{z} = \sqrt{P_v}\boldsymbol{\Phi}\mathbf{g} + \mathbf{z}, \quad (4)$$

where $\mathbf{g}_m = [g_m[0], \ldots, g_m[N_g - 1]]^T$, $\mathbf{z} = [z[0], \ldots, z[N_g + N_v + L - 3]]^T$, $\mathbf{H}_m$ is a Toeplitz matrix of size $(N_g + L - 1) \times N_g$ with the vector $[\mathbf{h}_m^T, \mathbf{0}^T]^T$ as its first column, and $\mathbf{V}$ is a Toeplitz matrix of size $(N_g + N_v + L - 2) \times (N_g + L - 1)$ with the vector $[\mathbf{v}^T, \mathbf{0}^T]^T$ as its first column. Besides, we define $\mathbf{g} = [\mathbf{g}_0^T, \ldots, \mathbf{g}_{M-1}^T]^T$ and $\boldsymbol{\Phi} = \mathbf{V}[\mathbf{H}_0, \ldots, \mathbf{H}_{M-1}]$. From (4), the energy delivery efficiency gain is computed as

$$\begin{aligned} E_G &= \frac{1}{N_v P_v}\mathbb{E}\left[\|\mathbf{y}\|_2^2\right] \\ &= \frac{1}{N_v P_v}\left(P_v\mathbf{g}^\dagger\boldsymbol{\Phi}^\dagger\boldsymbol{\Phi}\mathbf{g} + (N_g + N_v + L - 2)\cdot\sigma_z^2\right). \end{aligned} \quad (5)$$

The maximization problem for the energy delivery efficiency gain is then formulated as

$$\begin{aligned} (\mathbf{P1}):\ &\max_{\mathbf{g},\mathbf{v}}\ \mathbf{g}^\dagger\boldsymbol{\Phi}^\dagger\boldsymbol{\Phi}\mathbf{g} \\ &\text{s.t.} \quad (C.1) \quad \|\mathbf{g}\|_2^2 = 1; \\ &\qquad (C.2) \quad \|\mathbf{v}\|_2^2 = N_v. \end{aligned} \quad (6)$$

The joint design problem, however, is non-convex, which cannot be directly solved in its current form. To make the problem tractable, we propose an iterative method to handle the problem based on alternating optimization, in which the reference signal and the waveform are optimized and updated alternatively. For a given reference signal $\mathbf{v}$, the optimization problem for the waveform design is equivalent to an eigenvalue maximization problem; that is, the optimal waveform is given by

$$\hat{\mathbf{g}} = \boldsymbol{\zeta}_1\left[\boldsymbol{\Phi}^\dagger\boldsymbol{\Phi}\right]. \quad (7)$$

On the other hand, we can rewrite (3) as

$$\mathbf{y} = \sqrt{P_v}\sum_{m=0}^{M-1}\bar{\mathbf{H}}_m\mathbf{G}_m\mathbf{v} + \mathbf{z} = \sqrt{P_v}\bar{\boldsymbol{\Phi}}\mathbf{v} + \mathbf{z}, \quad (8)$$

where $\mathbf{G}_m$ is a Toeplitz matrix of size $(N_g + N_v - 1) \times N_v$ with the vector $[\mathbf{g}_m^T, \mathbf{0}^T]^T$ as its first column, $\bar{\mathbf{H}}_m$ is a Toeplitz matrix of size $(N_g + N_v + L - 2) \times (N_g + N_v - 1)$ with the vector $[\mathbf{h}_m^T, \mathbf{0}^T]^T$ as its first column, and $\bar{\boldsymbol{\Phi}} = \sum_{m=0}^{M-1}\bar{\mathbf{H}}_m\mathbf{G}_m$. As a result, for a given waveform $\mathbf{g}$, the optimization problem for designing the reference signal in (6) can be expressed as

$$\begin{aligned} (\mathbf{P2}):\ &\max_{\mathbf{v}}\ \mathbf{v}^\dagger\bar{\boldsymbol{\Phi}}^\dagger\bar{\boldsymbol{\Phi}}\mathbf{v} \\ &\text{s.t.} \quad (C.1) \quad \|\mathbf{v}\|_2^2 = N_v. \end{aligned} \quad (9)$$

Accordingly, the optimal reference signal is given by

$$\hat{\mathbf{v}} = \sqrt{N_v}\cdot\boldsymbol{\zeta}_1\left[\bar{\boldsymbol{\Phi}}^\dagger\bar{\boldsymbol{\Phi}}\right]. \quad (10)$$

An iterative algorithm for jointly optimizing the reference signal and the waveform is summarized in Table I, where

TABLE I
Iterative Algorithm for Finding the Reference Signal and Waveform

1: Set the iteration number $i = 0$ and the maximum allowable iteration number I_{max} ;
2: Initialize the reference signal $\mathbf{v}^{(i)}$;
3: **repeat**
4: For the given $\mathbf{v}^{(i)}$, compute the optimal waveform $\mathbf{g}^{(i)}$ using (7) ;
5: For the given $\mathbf{g}^{(i)}$, compute the optimal reference signal $\mathbf{v}^{(i+1)}$ using (10) ;
6: Set $i \leftarrow i + 1$;
7: **until** $\frac{1}{N_v}\left\|\mathbf{v}^{(i)} - \mathbf{v}^{(i-1)}\right\|_2^2 \le \varepsilon$ or $i \ge I_{max}$.

[‡]Another architecture is to apply different reference signals for the transmit antennas, or equivalently, to combine the reference signal and waveform at each antenna as one set of variables. This is just a special case of Fig. 1 by setting $N_v = 1$ and $v[0] = 1$ and treating $\mathbf{g}_m$ as the variable to be optimized. Based on our numerical simulations, this architecture performs worse than that adopted in Fig. 1.

[‖]Here we assume that the large-scale path loss is normalized and mainly address the gain that can be provided by the joint power waveforming and beamforming. The exact energy delivery efficiency is equal to the energy delivery efficiency gain minus the path loss (in dB).

the reference signal $\mathbf{v}$ and the waveform $\mathbf{g}$ are alternatively updated based on the latest value obtained at iteration. The procedures are repeated until a stopping criterion is met. The stopping criterion is to check whether $\frac{1}{N_v}\|\mathbf{v}^{(i)}-\mathbf{v}^{(i-1)}\|_2^2 \le \varepsilon$, where ε is a sufficiently small threshold, or the iteration number reaches a predefined limit $I_{\max}$. The convergence is analyzed as follows. Let $\Theta(\mathbf{v},\mathbf{g})$ be the optimal objective value of the problems (**P1**) or (**P2**). The sequence $\{\Theta(\mathbf{v}^{(i)},\mathbf{g}^{(i)})\}$ is increasing and bounded upper, since $\Theta(\mathbf{v}^{(i)},\mathbf{g}^{(i)}) \le \Theta(\mathbf{v}^{(i+1)},\mathbf{g}^{(i)}) \le \Theta(\mathbf{v}^{(i+1)},\mathbf{g}^{(i+1)})$. Therefore, the convergence of the algorithm is guaranteed. In addition, we evaluate the complexity of the proposed algorithm in terms of the required number of complex multiplications per iteration. Assume that the complexity of finding the principal eigenvector of an $N \times N$ matrix is N^3. The calculation of (7) and (10) involves the matrix-matrix products and the principal eigenvector of a matrix, and the total complexity per iteration is no more than $N_{max}^3(M^3+3M^2+12M+4)$. From (5) and (6), the achievable energy delivery efficiency gain is thus given by

$$E_G = \frac{1}{N_v P_v}\left(P_v \lambda_{\max}\left[\mathbf{\Phi}^{(i)\dagger}\mathbf{\Phi}^{(i)}\right] + (N_g+N_v+L-2)\,\sigma_z^2\right), \tag{11}$$

where $\mathbf{\Phi}^{(i)} = \mathbf{V}^{(i)}[\mathbf{H}_0,\ldots,\mathbf{H}_{M-1}]$, and the matrix $\mathbf{V}^{(i)}$ is obtained by substituting $\mathbf{v}^{(i)}$ into $\mathbf{V}$.

While the reference signal can be easily initialized by randomly generated complex binary signals, it is of great importance to carefully initialize the reference signal in order to achieve better WPT performance once the algorithm gets converged. To get more insight into determining a suitable initial value of $\mathbf{v}^{(0)}$, an example of the optimal waveform in the time domain, along with its relationship to the frequency-domain representations of $v[n]$, $g_m[n]$ and $h_m[n]$, is illustrated in Fig. 2 for a given reference signal, where $M=2$, $N_g=100$, $N_v=50$, and $P_v=1$. Here, a Saleh-Valenzuela (SV) channel model in [32] is adopted to generate the multipath channels. An $N_{\max}$-point DFT is performed for the spectrum analysis, where $N_{\max}=\max\{N_g,N_v,L\}$. Since the signals $v[n]$, $g_m[n]$ and $h_m[n]$ have different lengths, they are zero-padded when applying the $N_{\max}$-point DFT. The frequency-domain representations of $v[n]$, $g_m[n]$ and $h_m[n]$ are denoted as $\tilde{v}[k]$, $\tilde{g}_m[k]$ and $\tilde{h}_m[k]$, respectively, for $k=0,\ldots,N_{\max}-1$. Furthermore, we define $\tilde{q}[k]=|\tilde{v}[k]|^2\sum_{m=0}^{M-1}|\tilde{h}_m[k]|^2$, for $k=0,\ldots,N_{\max}-1$. Fig. 2(a) exemplifies the optimal waveform with respect to a randomly generated reference signal $v[n]$, whose time-domain and frequency-domain representations are given in Fig. 2(b) and Fig. 2(c), respectively. The optimal waveforms for the two transmit antennas in the frequency domain are shown in Fig. 2(d) and Fig. 2(e) respectively, and we can make two interesting observations. First, the waveforms both concentrate its allocated power on a peak frequency tone $k=94$ with the largest value of $\tilde{q}[k]$. Second, at different antennas, the larger the value of $|\tilde{h}_m[k]|^2|\tilde{v}[k]|^2$ at the peak frequency tone $k=94$, the more power the waveform is allocated.

From the first observation, the waveforms bear resemblance to single tones with the same frequency, and thus, the received power is in a specific formula. This motivates the initialization format of $\mathbf{v}^{(0)}$ by condensing the power spectrum of the initial reference signal into a frequency tone with the largest value of the summation of the channel power over all the antennas, i.e., $\sum_{m=0}^{M-1}|\tilde{h}_m[k]|^2$, in order to maximize the peak value of $\tilde{q}[k]$. By doing so, the nth entry of the initial reference signal $\mathbf{v}^{(0)}$ is given as

$$v^{(0)}[n] = e^{j\frac{2\pi k_{\max} n}{N_{\max}}},\quad n=0,\ldots,N_v-1, \tag{12}$$

where $k_{\max}=\arg\max_{k=0,\ldots,N_{\max}-1}\sum_{m=0}^{M-1}|\tilde{h}_m[k]|^2$. Another reason is that since $\mathbf{g}_m$ is unknown at the initialization stage, by assuming that $\mathbf{g}_m=\mathbf{e}_1$, for all m, the received signal is reduced to $\mathbf{y}=\sqrt{P_v}\sum_{m=0}^{M-1}\bar{\mathbf{H}}_m\mathbf{v}+\mathbf{z}$. From the frequency-domain viewpoint, the received signal is the multiplication between $\tilde{v}[k]$ and $\tilde{h}_m[k]$, and hence, the reference signal in (12) is a good initial choice. It is noted that the proposed initial reference signal is equivalent to a complex sinusoidal signal truncated by a rectangular window to a length of N_v; hence, its frequency-domain representation is essentially a sinc function centered at the $k_{\max}^{\text{th}}$ frequency tone.

B. Waveform Design With Periodic Reference Signals

In this subsection, we investigate the optimal waveform design when the reference signal $v[n]$ is periodically transmitted over time, i.e., $v[n]=v[n+N_v]$. From (3), since $v[n]$ is N_v-periodic, the received signal at the receiver side is also N_v-periodic, given by

$$\mathbf{y}_c = \sqrt{P_v}\sum_{m=0}^{M-1}\mathbf{R}\mathbf{H}_m\mathbf{g}_m + \mathbf{z}_c, \tag{13}$$

where $\mathbf{y}_c=[y[0],\ldots,y[N_v-1]]^T$, $\mathbf{z}_c=[z[0],\ldots,z[N_v-1]]^T$, $\mathbf{R}$ is a generalized circulant matrix of size $N_v\times(N_g+L-1)$, whose jth column is the cyclic permutation of the vector $\mathbf{v}$ with an offset $((j))_{N_v}$, for $j=0,\ldots,N_g+L-2$. By defining $\mathbf{\Phi}_c=\mathbf{R}[\mathbf{H}_0,\ldots,\mathbf{H}_{M-1}]$, we can rewrite (13) into a compact matrix-vector form:

$$\mathbf{y}_c = \sqrt{P_v}\mathbf{\Phi}_c\mathbf{g}+\mathbf{z}. \tag{14}$$

According to Definition 1, if the transmission time is sufficiently large, the energy delivery efficiency gain can be approximated as

$$E_{c,G} = \frac{1}{N_v P_v}\mathbb{E}\left[\|\mathbf{y}_c\|_2^2\right] = \frac{1}{N_v P_v}\left(P_v\mathbf{g}^\dagger\mathbf{\Phi}_c^\dagger\mathbf{\Phi}_c\mathbf{g}+N_v\sigma_z^2\right). \tag{15}$$

Under a given reference signal, the optimal waveform for maximizing the energy delivery efficiency gain in (15) can be computed as

$$\hat{\mathbf{g}}_c = \boldsymbol{\zeta}_1\left[\mathbf{\Phi}_c^\dagger\mathbf{\Phi}_c\right], \tag{16}$$

where $\hat{\mathbf{g}}_c=[\hat{\mathbf{g}}_{c,0},\ldots,\hat{\mathbf{g}}_{c,M-1}]^T$. Similar to the previous subsection, the reference signal and waveforms in the case of periodic transmission can be jointly optimized by following similar

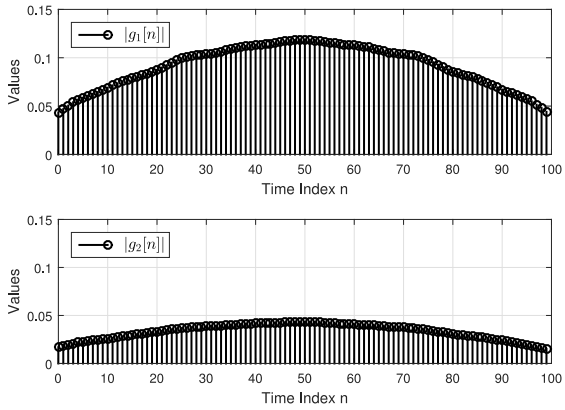

(a) The values of $|g_1[n]|$ and $|g_2[n]|$

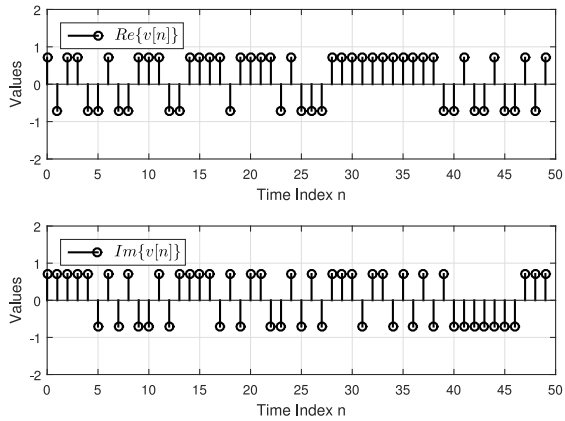

(b) Real and imaginary parts of $v[n]$

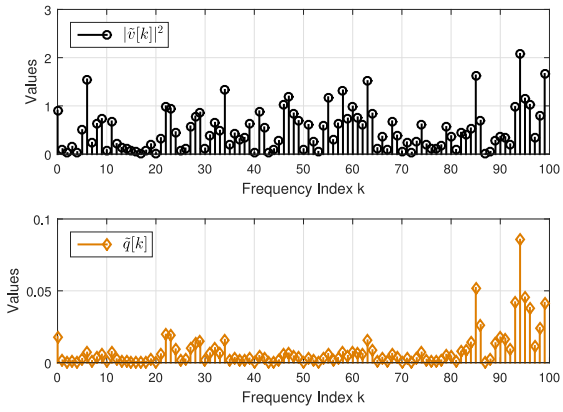

(c) The values of $|\tilde{v}[k]|^2$ and $\tilde{q}[k]$

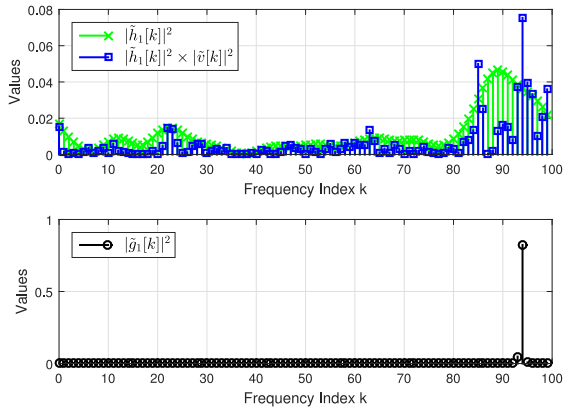

(d) The values of $\left|\tilde{h}_1[k]\right|^2$, $\left|\tilde{h}_1[k]\right|^2|\tilde{v}[k]|^2$ and $|\tilde{g}_1[k]|^2$

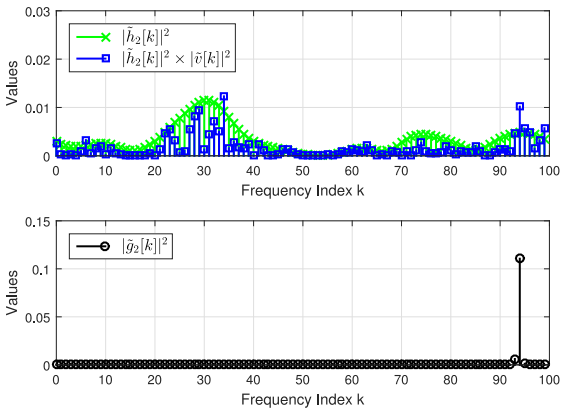

(e) The values of $\left|\tilde{h}_2[k]\right|^2$, $\left|\tilde{h}_2[k]\right|^2|\tilde{v}[k]|^2$ and $|\tilde{g}_2[k]|^2$

Fig. 2. An example of the optimal waveform in the time domain and the frequency domain, along with its relationship to $|\tilde{h}_m[k]|^2$, $|\tilde{v}[k]|^2$ and $\tilde{q}[k]$, for a given reference signal ($M = 2$, $N_g = 100$, $N_v = 50$, and $P_v = 1$).

iterative steps in Table I. Due to the limited space, the detailed derivation of the optimal reference signal for given waveforms is omitted here.

According to (14), let $\mathbf{\Phi}_{c,m} = \mathbf{R}\mathbf{H}_m$ be the mth submatrix of $\mathbf{\Phi}_c$, which is also a generalized circulant matrix of size $N_v \times N_g$. We define the first column of the matrix $\mathbf{\Phi}_{c,m}$ as $\boldsymbol{\phi}_m$, for $m = 0, \ldots, M-1$, and its frequency representation as $\tilde{\boldsymbol{\phi}}_m = [\tilde{\phi}_m[0], \ldots, \tilde{\phi}_m[N_v - 1]]^T = \mathbf{F}_{N_v}\boldsymbol{\phi}_m$. From (15), the energy delivery efficiency gain is upper bounded by

$$\begin{aligned} E_{c,G} &\leq \tfrac{1}{N_v P_v}\left(P_v \|\mathbf{\Phi}_c\|_2^2 + N_v\sigma_z^2\right) \\ &= \tfrac{1}{N_v P_v}\left(P_v \lambda_{\max}\left[\mathbf{\Phi}_c^\dagger \mathbf{\Phi}_c\right] + N_v\sigma_z^2\right) \\ &= \tfrac{1}{N_v P_v}\left(P_v \lambda_{\max}\left[\mathbf{\Phi}_c \mathbf{\Phi}_c^\dagger\right] + N_v\sigma_z^2\right) \\ &= \tfrac{1}{N_v P_v}\left(P_v \lambda_{\max}\left[\sum_{m=0}^{M-1} \mathbf{\Phi}_{c,m}\mathbf{\Phi}_{c,m}^\dagger\right] + N_v\sigma_z^2\right), \end{aligned} \quad (17)$$

where the relationship of $\|\mathbf{\Phi}_c\mathbf{g}\|_2^2 \le \|\mathbf{\Phi}_c\|_2^2\|\mathbf{g}\|_2^2$ and $\|\mathbf{g}\|_2^2 = 1$ is applied to the first inequality. Let $\bar{\mathbf{\Phi}}_{c,m}$ be an $N_v \times N_v$ circulant matrix with $\boldsymbol{\phi}_m$ as its first column, and we have $\mathbf{F}_{N_v}\bar{\mathbf{\Phi}}_{c,m}\mathbf{F}_{N_v}^{\dagger} = \sqrt{N_v}Diag[\tilde{\boldsymbol{\phi}}_m]$. Since $N_g = QN_v$, it can be shown from (13) that $\mathbf{\Phi}_{c,m} = \mathbf{R}\mathbf{H}_m = \mathbf{1}_Q^T \otimes \bar{\mathbf{\Phi}}_{c,m}$, yielding $\mathbf{F}_{N_v}\mathbf{\Phi}_{c,m}(\mathbf{I}_Q \otimes \mathbf{F}_{N_v})^{\dagger} = \sqrt{N_v}(\mathbf{1}_Q^T \otimes Diag[\tilde{\boldsymbol{\phi}}_m])$. By using the property of $\mathbf{F}_{N_v}\mathbf{F}_{N_v}^{\dagger} = \mathbf{F}_{N_v}^{\dagger}\mathbf{F}_{N_v} = \mathbf{I}_{N_v}$ and inserting the DFT matrix into (17), one can diagonalize the matrix $\mathbf{\Phi}_{c,m}$ as shown in (19) shown at the bottom of this page. Since $\lambda_{\max}[\sum_{m=0}^{M-1} Diag[\tilde{\boldsymbol{\phi}}_m] \cdot Diag[\tilde{\boldsymbol{\phi}}_m]^{\dagger}] = \sum_{m=0}^{M-1}\left|\tilde{\phi}_m[k_{c,\max}]\right|^2$, the energy delivery efficiency gain in (19) is finally bounded by

$$E_{c,G} \le Q \cdot \sum\nolimits_{m=0}^{M-1}\left|\tilde{\phi}_m\left[k_{c,\max}\right]\right|^2 + \frac{\sigma_z^2}{P_v}, \tag{18}$$

where $k_{c,\max} = \arg\max_{k=0,\ldots,N_v-1}\sum_{m=0}^{M-1}\left|\tilde{\phi}_m[k]\right|^2$.

Below we are interested in discovering the structure of the optimal waveform and reference signal. In fact, it can be proved that with the periodic transmission of a reference signal, the optimal waveform for each transmit antenna in (16) is endowed with a simple single-tone structure, if the lengths of the waveform and the reference signal are appropriately designed. The following theorem is then provided.

Theorem 1: Let $N_g = Q \cdot N_v$, where Q is a positive integer. For any reference signal $\mathbf{v}$, the optimal waveforms $\hat{\mathbf{g}}_{c,m}$ at transmit antennas are single-tone waveforms, given by

$$\hat{\mathbf{g}}_{c,m} = \frac{\tilde{\phi}_m^*\left[k_{c,\max}\right]}{\sqrt{\sum_{m=0}^{M-1}\left|\tilde{\phi}_m\left[k_{c,\max}\right]\right|^2}}\left(\frac{1}{\sqrt{Q}}\mathbf{1}_Q \otimes \left(\mathbf{F}_{N_v}^{\dagger}\mathbf{e}_{k_{c,\max}}\right)\right), \quad m = 0,\ldots,M-1, \tag{21}$$

with $k_{c,\max} = \arg\max_{k=0,\ldots,N_v-1}\sum_{m=0}^{M-1}\left|\tilde{\phi}_m[k]\right|^2$.

Proof: To prove this theorem, we show that the proposed optimal waveform in (21) can achieve the upper bound in (18). Substituting (21) into (15), we can obtain (20) shown at the bottom of this page, where the third equality is obtained by inserting the DFT matrix $\mathbf{F}_{N_v}$. By applying the result of $\mathbf{F}_{N_v}\mathbf{\Phi}_{c,m}(\mathbf{1}_Q \otimes (\mathbf{F}_{N_v}^{\dagger}\mathbf{e}_{k_{c,\max}})) = Q\sqrt{N_v}\tilde{\phi}_m[k_{c,\max}]\mathbf{e}_{k_{c,\max}}$ into (20), it then yields

$$E_{c,G} = Q \cdot \sum_{m=0}^{M-1}\left|\tilde{\phi}_m\left[k_{c,\max}\right]\right|^2 + \frac{\sigma_z^2}{P_v}. \tag{22}$$

The proof is thus completed. ■

From Theorem 1, it can be found that if the waveform length is a multiple of the length of the reference signal, the optimal waveform $\hat{\mathbf{g}}_{c,m}$ is a complex sinusoidal signal, merely composed of a single frequency component $k_{c,\max}$, no matter what the reference signal is. Moreover, the term $\tilde{\phi}_m^*[k_{c,\max}]$ represents a power allocation and phase alignment factor for the mth transmit antenna, while the term $\frac{1}{\sqrt{\sum_{m=0}^{M-1}\left|\tilde{\phi}_m\left[k_{c,\max}\right]\right|^2}}$ is a power normalization factor. This simple structure offers an attractive solution for low-complexity implementation of the optimal waveform without the need of executing eigenvalue decomposition, as compared with (7) and (16). Based on Theorem 1, two corollaries regarding the achievable energy delivery efficiency gain and the effect of the waveform length on the WPT performance are provided in the following.

Corollary 1: When $N_g = Q \cdot N_v$, where Q is a positive integer, the energy delivery efficiency gain achieved by the optimal single-tone waveform $\hat{\mathbf{g}}_{c,m}$ in (21) is

$$E_{c,G} = Q \cdot \sum\nolimits_{m=0}^{M-1}\left|\tilde{\phi}_m\left[k_{c,\max}\right]\right|^2 + \frac{\sigma_z^2}{P_v}. \tag{23}$$

Proof: This result is directly obtained from (22). ■

Corollary 2: Let J be a positive integer. When $\frac{\sigma_z^2}{P_v}$ approaches to zero, the energy delivery efficiency gain with respect to the optimal single-tone waveform $\hat{\mathbf{g}}_{c,m}$ in (21) can be

$$\begin{aligned} E_{c,G} &\le \frac{1}{N_v P_v}\left(P_v\lambda_{\max}\left[\sum\nolimits_{m=0}^{M-1}\mathbf{F}_{N_v}\mathbf{\Phi}_{c,m}(\mathbf{I}_Q \otimes \mathbf{F}_{N_v})^{\dagger}(\mathbf{I}_Q \otimes \mathbf{F}_{N_v})\mathbf{\Phi}_{c,m}^{\dagger}\mathbf{F}_{N_v}^{\dagger}\right] + N_v\sigma_z^2\right) \\ &= \frac{1}{N_v P_v}\left(N_v Q P_v \cdot \lambda_{\max}\left[\sum\nolimits_{m=0}^{M-1} Diag\left[\tilde{\boldsymbol{\phi}}_m\right] \cdot Diag\left[\tilde{\boldsymbol{\phi}}_m\right]^{\dagger}\right] + N_v\sigma_z^2\right). \end{aligned} \tag{19}$$

$$\begin{aligned} E_{c,G} &= \frac{1}{N_v P_v}\left(P_v\left\|\sum\nolimits_{m=0}^{M-1}\mathbf{\Phi}_{c,m}\mathbf{g}_{c,m}\right\|_2^2 + N_v\sigma_z^2\right) \\ &= \frac{1}{N_v P_v}\left(P_v\left\|\sum_{m=0}^{M-1}\mathbf{\Phi}_{c,m}\frac{\tilde{\phi}_m^*\left[k_{c,\max}\right]}{\sqrt{\sum_{m=0}^{M-1}\left|\tilde{\phi}_m\left[k_{c,\max}\right]\right|^2}}\left(\frac{1}{\sqrt{Q}}\mathbf{1}_Q \otimes \left(\mathbf{F}_{N_v}^{\dagger}\mathbf{e}_{k_{c,\max}}\right)\right)\right\|_2^2 + N_v\sigma_z^2\right) \\ &= \frac{1}{N_v P_v}\left(P_v\left\|\mathbf{F}_{N_v}\sum_{m=0}^{M-1}\mathbf{\Phi}_{c,m}\frac{\tilde{\phi}_m^*\left[k_{c,\max}\right]}{\sqrt{\sum_{m=0}^{M-1}\left|\tilde{\phi}_m\left[k_{c,\max}\right]\right|^2}}\left(\frac{1}{\sqrt{Q}}\mathbf{1}_Q \otimes \left(\mathbf{F}_{N_v}^{\dagger}\mathbf{e}_{k_{c,\max}}\right)\right)\right\|_2^2 + N_v\sigma_z^2\right), \end{aligned} \tag{20}$$

approximately improved by J times, if the waveform length N_g is prolonged by J times.

Proof: Consider two waveform lengths $N_{g,1} = Q \cdot N_v$ and $N_{g,2} = J \cdot N_{g,1}$. The energy delivery efficiency gains for the optimal single-tone waveform designs with the length $N_{g,1}$ and $N_{g,2}$ are denoted as E_{c,G_1} and E_{c,G_2}, respectively. From Corollary 1, we have

$$\frac{E_{c,G_2}}{E_{c,G_1}} = \frac{JQN_v \sum_{m=0}^{M-1} \left|\tilde{\phi}_m\left[k_{c,\max}\right]\right|^2 + \frac{\sigma_z^2}{P_v}}{QN_v \sum_{m=0}^{M-1} \left|\tilde{\phi}_m\left[k_{c,\max}\right]\right|^2 + \frac{\sigma_z^2}{P_v}}. \tag{24}$$

If $\frac{\sigma_z^2}{P_v}$ is sufficiently small, the above ratio can be approximated as

$$\frac{E_{c,G_2}}{E_{c,G_1}} \approx J. \tag{25}$$

■

From Corollary 1 and Corollary 2, it is found that the energy delivery efficiency gain achieved by the optimal single-tone waveform can be linearly increased by enlarging the waveform length, if $\frac{\sigma_z^2}{P_v}$ is sufficiently small. In general, this condition is true because the transmit power P_v is much larger than the noise power σ_z^2 in the WPT applications. Also the performance gain is determined by $\sum_{m=0}^{M-1} |\tilde{\phi}_m[k_{c,\max}]|^2$, which is related to the frequency selectivity of the wireless channels and the reference signal.

In what follows, we investigate the design structure of the optimal reference signal. Let $\tilde{\mathbf{h}}_m = [\tilde{h}_m[0], \ldots, \tilde{h}_m[N_v - 1]]^T = \mathbf{F}_{N_v} \bar{\mathbf{h}}_m$, where $\bar{\mathbf{h}}_m = [\mathbf{h}_m^T, \mathbf{0}^T]^T$, and define $\bar{\mathbf{R}}$ as a circulant matrix whose first column is $\mathbf{v}$. A theorem regarding the optimal reference signal is provided in the following.

Theorem 2: When $N_v \geq L$, the optimal reference signal for the multi-antenna PW system with periodic transmission is given by

$$\hat{v}[n] = e^{j\frac{2\pi k_{c,\max} n}{N_v}}, \quad n = 0, \ldots, N_v - 1, \tag{26}$$

where $k_{c,\max} = \arg \max_{k=0,\ldots,N_v-1} \sum_{m=0}^{M-1} |\tilde{h}_m[k]|^2$.

Proof: By the definition of $\mathbf{\Phi}_{c,m} = \mathbf{R}\mathbf{H}_m = \mathbf{1}_Q^T \otimes \bar{\mathbf{\Phi}}_{c,m}$ in (17), we have $\boldsymbol{\phi}_m = \bar{\mathbf{R}}\bar{\mathbf{h}}_m$, if $N_v \geq L$. Hence, it implies $\tilde{\boldsymbol{\phi}}_m = \mathbf{F}_{N_v}\boldsymbol{\phi}_m = \mathbf{F}_{N_v}\bar{\mathbf{R}}\bar{\mathbf{h}}_m$. By diagonalizing $\bar{\mathbf{R}}$, it further gives

$$\tilde{\boldsymbol{\phi}}_m = \mathbf{F}_{N_v}\bar{\mathbf{R}}\mathbf{F}_{N_v}^{\dagger}\mathbf{F}_{N_v}\bar{\mathbf{h}}_m = \sqrt{N_v}\,Diag\left[\tilde{\mathbf{v}}\right]\tilde{\mathbf{h}}_m, \tag{27}$$

where $\tilde{\mathbf{v}} = \mathbf{F}_{N_v}\mathbf{v}$. By using (27), we can obtain

$$\begin{aligned}\tilde{\boldsymbol{\phi}}_m \odot \tilde{\boldsymbol{\phi}}_m^* &= Diag\left[\sqrt{N_v}Diag\left[\tilde{\mathbf{v}}\right]\tilde{\mathbf{h}}_m\right] \cdot \sqrt{N_v}Diag\left[\tilde{\mathbf{v}}\right]^*\tilde{\mathbf{h}}_m^* \\ &= N_v Diag\left[\tilde{\mathbf{v}}\right] \cdot Diag[\tilde{\mathbf{v}}]^* \cdot Diag\left[\tilde{\mathbf{h}}_m\right] \cdot \tilde{\mathbf{h}}_m^* \\ &= N_v\left(\tilde{\mathbf{v}} \odot \tilde{\mathbf{v}}^*\right) \odot \left(\tilde{\mathbf{h}}_m \odot \tilde{\mathbf{h}}_m^*\right).\end{aligned} \tag{28}$$

From Corollary 1, it is known that the optimal reference signal can be found by maximizing $E_{c,G}$ in (23), or equivalently, maximizing $\sum_{m=0}^{M-1} |\tilde{\phi}_m[k_{c,\max}]|^2$. Since $\sum_{m=0}^{M-1} \tilde{\boldsymbol{\phi}}_m \odot \tilde{\boldsymbol{\phi}}_m^* = \sum_{m=0}^{M-1} [|\tilde{\phi}_m[0]|^2, \ldots, |\tilde{\phi}_m[N_v-1]|^2]^T$, the energy delivery efficiency gain can be maximized by letting $\tilde{\mathbf{v}} = \sqrt{N_v}\mathbf{e}_{k_{c,\max}}$, where $k_{c,\max} = \arg \max_{k=0,\ldots,N_v-1} \sum_{m=0}^{M-1} |\tilde{h}_m[k]|^2$. The optimal reference signal in the time domain is thus given by $\hat{\mathbf{v}} = \mathbf{F}_{N_v}^{\dagger}\tilde{\mathbf{v}} = \sqrt{N_v}\mathbf{F}_{N_v}^{\dagger}\mathbf{e}_{k_{c,\max}}$. ■

Theorem 2 implies that for the scenario of periodic transmission, the optimal reference signal is indeed a complex sinusoidal signal when $N_v \geq L$[¶]. Also from (27) and (28) in the proof of this theorem, we can get $\tilde{\phi}_m[k] = N_v\tilde{h}_m[k]$ and $|\tilde{\phi}_m[k]|^2 = N_v^2|\tilde{h}_m[k]|^2$, for $k = 0, \ldots, N_v - 1$, since $\tilde{\mathbf{v}} = \sqrt{N_v}\mathbf{e}_{k_{c,\max}}$. By using Theorem 1, the optimal waveform, associated with the optimal reference signal, can be explicitly expressed as

$$\hat{\mathbf{g}}_{c,m} = \frac{\tilde{h}_m^*\left[k_{c,\max}\right]}{\sqrt{\sum_{m=0}^{M-1}\left|\tilde{h}_m\left[k_{c,\max}\right]\right|^2}}\left(\frac{1}{\sqrt{Q}}\mathbf{1}_Q \otimes \left(\mathbf{F}_{N_v}^{\dagger}\mathbf{e}_{k_{c,\max}}\right)\right), \quad m = 0, \ldots, M-1. \tag{29}$$

Corollary 3: When $N_g = Q \cdot N_v$ and $N_v \geq L$, the energy delivery efficiency gain for the optimal reference signal in (26) and the corresponding optimal waveform in (29) is given by

$$E_{c,G} = N_g N_v \cdot \sum_{m=0}^{M-1}\left|\tilde{h}_m\left[k_{c,\max}\right]\right|^2 + \frac{\sigma_z^2}{P_v}. \tag{30}$$

Proof: By using $\left|\tilde{\phi}_m\left[k\right]\right|^2 = N_v^2\left|\tilde{h}_m\left[k\right]\right|^2$ and from Corollary 1, the energy delivery efficiency gain can be derived as $E_{c,G} = QN_v^2 \sum_{m=0}^{M-1} \cdot \left|\tilde{h}_m\left[k_{c,\max}\right]\right|^2 + \frac{\sigma_z^2}{P_v}$. The proof is thus completed. ■

It is addressed by this corollary that under the mentioned conditions and optimal designs, the energy delivery efficiency gain is appropriately proportional to the product of the lengths of the waveform and reference signal, if $\frac{\sigma_z^2}{P_v}$ is small enough.

IV. Performance Analysis of Multi-antenna PW Systems

In this section, we theoretically analyze the WPT performance of the proposed multi-antenna PW system. It is tough to analyze the WPT performance under the case of the non-periodic transmissions of reference signals. Alternatively, the WPT performance is investigated under the case of the periodic transmissions of reference signals. In addition to the average energy delivery efficiency gain, an outage probability of the average harvested energy, which is different from the conventional notation used in wireless information transmission, is taken into consideration to quantify the performance. Specifically, the outage event is defined as follows.

Definition 2: A multi-antenna PW system is in outage, if the harvested energy is smaller than or equal to a preset threshold x.

To make the analysis tractable, it is assumed that $N_g = Q \cdot N_v$ and $N_v = C \cdot L$ throughout this section, where Q and

[¶]The complex sinusoidal structure of the optimal reference signal depends on the considered periodic or non-periodic scenarios, together with the conditions $N_g = QN_v$ and $N_v \geq L$.

C both take positive integer values. For the WPT applications, this is true because the lengths of the waveforms and the reference signal are in general larger than the channel length in order to achieve a higher energy delivery efficiency gain, as shown in (30). Moreover, it is almost impossible to analyze the performance for general channel power delay profiles; instead, we consider a uniform power delay (UPD) channel profile, i.e., $\rho_{m,l} = \frac{1}{L}$ in (1), and investigate the impact of the numbers of multipaths and antennas on the WPT performance. From Corollary 3, one can observe that both the average energy delivery efficiency gain and the outage performance of the average harvested energy are mainly influenced by the channel frequency selective fading effect $\sum_{m=0}^{M-1}\left|\tilde{h}_m\left[k_{c,\max}\right]\right|^2$. To facilitate the analysis, a performance lower bound for the energy delivery efficiency gain in (30) under the UPD channel profile is given in the following lemma.

Lemma 1: When $N_g = Q \cdot N_v$ and $N_v = C \cdot L$, the energy delivery efficiency gain for the optimal reference signal in (26) and the corresponding optimal waveform in (29) under the UPD channel profile can be lower bounded by

$$E_{c,G} \geq N_g L \sum\nolimits_{m=0}^{M-1}\left|\tilde{u}_m\left[k_{c,\max}\right]\right|^2 + \frac{\sigma_z^2}{P_v}, \tag{31}$$

where $\tilde{\mathbf{u}}_m = \left[\tilde{u}_m\left[0\right],\ldots,\tilde{u}_m\left[L-1\right]\right]^T = \mathbf{F}_L\mathbf{h}_m$, and $k_{c,\max} = \arg\max_{k=0,\ldots,L-1}\sum_{m=0}^{M-1}\left|\tilde{u}_m\left[k\right]\right|^2$. Moreover, the equality in (31) holds for $C=1$ or $L=1$.

Proof: From the definition of $\tilde{\mathbf{h}}_m = \mathbf{F}_{N_v}\bar{\mathbf{h}}_m$ and $N_v = C\cdot L$, it gives

$$\tilde{h}_m\left[Ck+l\right] = \sqrt{\frac{L}{N_v}}\left(\frac{1}{\sqrt{L}}\sum_{n=0}^{L-1}h_m\left[n\right]e^{-j\frac{2\pi kn}{L}}e^{-j\frac{2\pi ln}{N_v}}\right),$$
$$k=0,\ldots,L-1, l=0,\ldots,C-1. \tag{32}$$

By using $\tilde{\mathbf{u}}_m = \mathbf{F}_L\mathbf{h}_m$, we can obtain the relationship between $\tilde{h}_m\left[k\right]$ and $\tilde{u}_m\left[k\right]$:

$$\tilde{h}_m\left[Ck\right] = \sqrt{\frac{L}{N_v}}\tilde{u}_m\left[k\right], \quad k=0,\ldots,L-1. \tag{33}$$

It then implies from (33) that

$$\begin{aligned}\max_{k=0,\ldots,N_v-1}&\sum\nolimits_{m=0}^{M-1}\left|\tilde{h}_m\left[k\right]\right|^2\\ &\geq \max_{k=0,\ldots,L-1}\sum\nolimits_{m=0}^{M-1}\left|\tilde{h}_m\left[Ck\right]\right|^2\\ &= \max_{k=0,\ldots,L-1}\frac{L}{N_v}\sum\nolimits_{m=0}^{M-1}\left|\tilde{u}_m\left[k\right]\right|^2,\end{aligned} \tag{34}$$

where the inequality in (34) becomes active for $C=1$. Note that for $L=1$, the inequality is also active because $\left|\tilde{h}_m\left[k\right]\right|^2 = \frac{1}{N_v}\left|h_m\left[0\right]\right|^2$ for all k according to (32). From Corollary 3 and (34), the proof is thus completed. ■

From Lemma 1, it is found that the performance lower bound is relevant to the maximum value of $\sum_{m=0}^{M-1}\left|\tilde{u}_m\left[k\right]\right|^2$, which is the summation of the power of the L-point channel frequency responses over transmit antennas. Furthermore, this lower bound is reached when the length of the reference signal is identical to the number of multipaths or the number of multipaths for each channel link is equal to one. For the convenience of notation, let $\mu_k = \sum_{m=0}^{M-1}\left|\tilde{u}_m\left[k\right]\right|^2$, for $k=0,\ldots,L-1$, and $\boldsymbol{\mu} = \left[\mu_0,\ldots,\mu_{L-1}\right]^T$. The characteristic function of the multivariate random vector $\boldsymbol{\mu}$ is provided as follows.

Lemma 2: Let $\boldsymbol{\omega} = \left[\omega_0,\ldots,\omega_{L-1}\right]^T$. The characteristic function of $\boldsymbol{\mu}$ under the UPD channel profile is

$$\Psi_{\boldsymbol{\mu}}\left(j\boldsymbol{\omega}\right) = \left(\prod\nolimits_{l=0}^{L-1}\frac{L}{L-j\omega_l}\right)^M. \tag{35}$$

Proof: Let $\boldsymbol{\mu}_m = \left[\mu_{m,0},\ldots,\mu_{m,L-1}\right]^T$, where we define $\mu_{m,k} = \left|\tilde{u}_m\left[k\right]\right|^2$. From the proof of Theorem 5 in [27], the characteristic function of $\boldsymbol{\mu}_m$ under the UPD channel profile can be derived as

$$\Psi_{\boldsymbol{\mu}_m}\left(j\boldsymbol{\omega}\right) = \prod_{l=0}^{L-1}\frac{L}{L-j\omega_l}. \tag{36}$$

Since the random vectors $\boldsymbol{\mu}_m$ are independent for different transmit antennas and $\boldsymbol{\mu} = \sum_{m=0}^{M-1}\boldsymbol{\mu}_m$, it results in $\Psi_{\boldsymbol{\mu}}\left(j\boldsymbol{\omega}\right) = \prod_{m=0}^{M-1}\Psi_{\boldsymbol{\mu}_m}\left(j\boldsymbol{\omega}\right)$. Hence, the proof is completed. ■

By applying (15) and Lemma 1, the average harvested energy during a time period of N_v can be explicitly computed by $E_H \triangleq \frac{1}{N_v}\mathbb{E}\left[\left\|\mathbf{y}_c\right\|_2^2\right] = P_v E_{c,G}$, and thus, it is lower bounded by

$$E_H \geq N_g P_v L\cdot\mu_{k_{c,\max}} + \sigma_z^2. \tag{37}$$

Accordingly, a theorem regarding an upper bound for the outage performance of the average harvested energy is provided in the following.

Theorem 3: When $N_g = Q\cdot N_v$ and $N_v = C\cdot L$, the outage performance of the average harvested energy E_H for the optimal reference signal in (26) and the corresponding optimal waveform in (29) under the UPD channel profile is upper bounded by

$$\Pr(E_H \leq x) \leq \left(\frac{1}{(M-1)!}\cdot\gamma\left(M, \frac{1}{N_g P_v}\left(x-\sigma_z^2\right)\right)\right)^L, \tag{38}$$

where $\gamma\left(s,x\right) = \int_0^x t^{s-1}e^{-t}dt$ is the lower incomplete Gamma function, and the equality of the upper bound holds for $C=1$ or $L=1$.

Proof: By applying the characteristic function in (35), the cumulative distribution function (CDF) of $\boldsymbol{\mu}$ can be expressed in terms of $\Psi_{\boldsymbol{\mu}}\left(j\boldsymbol{\omega}\right)$ as follows [33]:

$$\begin{aligned}&\Pr\left(\mu_0\leq x_0,\mu_1\leq x_1,\ldots,\mu_{L-1}\leq x_{L-1}\right)\\ &\quad= \frac{1}{(2\pi)^L}\int_{-\infty}^{\infty}\cdots\int_{-\infty}^{\infty}\Psi_{\boldsymbol{\mu}}\left(j\boldsymbol{\omega}\right)\times\prod\nolimits_{l=0}^{L-1}\left(\frac{1-e^{-j\omega_l x_l}}{j\omega_l}\right)\\ &\qquad d\omega_0\cdots d\omega_{L-1},\end{aligned} \tag{39}$$

where $\mathbf{x} = \left[x_0,\ldots,x_{L-1}\right]^T$. Since $\mu_{k_{c,\max}} = \max_{k=0,\ldots,L-1}\mu_k$, the CDF of the random variable $\mu_{k_{c,\max}}$ is obtained by setting $x_0 =$

$\cdots = x_{L-1} = x$ in (39):

$$\Pr\left(\mu_{k_{c,\max}} \le x\right) = \frac{1}{(2\pi)^L}\int_{-\infty}^{\infty}\cdots\int_{-\infty}^{\infty}\Psi_{\boldsymbol{\mu}}\left(j\boldsymbol{\omega}\right) \times \prod_{l=0}^{L-1}\left(\frac{1-e^{-j\omega_l x}}{j\omega_l}\right)d\omega_0\cdots d\omega_{L-1}. \quad (40)$$

From (35) and (40), the CDF of the random variable $\mu_{k_{c,\max}}$ can be explicitly derived as shown in (41) shown at the bottom of this page. where the relationship between the CDF function and the characteristic function of the Erlang distribution is applied in the last equality of (41) as follows:

$$\frac{1}{2\pi}\int_{-\infty}^{\infty}\left(\frac{\beta}{\beta-j\omega}\right)^M\left(\frac{1-e^{-j\omega x}}{j\omega}\right)d\omega = \frac{1}{(M-1)!}\cdot\gamma\left(M,\beta x\right), \quad (43)$$

where $\gamma(s,x) = \int_0^x t^{s-1}e^{-t}dt$ is the lower incomplete Gamma function. By using (37), the outage performance of the average harvested energy E_H is upper bounded by

$$\Pr\left(E_H \le x\right) \le \Pr\left(N_g P_v L\cdot\mu_{k_{c,\max}} + \sigma_z^2 \le x\right). \quad (44)$$

From (41) and (44), it is concluded that the upper bound of the outage performance is given as in (38), and by further applying Lemma 1, we know that the upper bound becomes tight for $C = 1$ or $L = 1$. ■

Theorem 4: When $N_g = Q\cdot N_v$ and $N_v = C\cdot L$, the average energy delivery efficiency gain for the optimal reference signal in (26) and the corresponding optimal waveform in (29) under the UPD channel profile is lower bounded as shown in (42) shown at the bottom of this page in which $b_k\left(M,L,l\right)$ is the coefficient of x^k, for $k = 0,\ldots,(M-1)l$, in the expansion of

$$\left(\sum_{k=0}^{M-1}\frac{L^k x^k}{k!}\right)^l, \quad (45)$$

and $\binom{n}{k} = \frac{n!}{k!(n-k)!}$.

Proof: The lower incomplete Gamma function in (41) can be expressed in a form of power series expansion [34]:

$$\gamma\left(M,Lx\right) = \Gamma\left(M\right)\cdot\left(1-e^{-Lx}\sum_{k=0}^{M-1}\frac{L^k x^k}{k!}\right), \quad (46)$$

where $\Gamma(M) = (M-1)!$ is the Gamma function. Since $\mu_{k_{c,\max}} \ge 0$, the mean of the random variable $\mu_{k_{c,\max}}$ can be directly computed through its CDF as follows:

$$\mathbb{E}\left[\mu_{k_{c,\max}}\right] = \int_0^{\infty}\left(1-\Pr\left(\mu_{k_{c,\max}} \le x\right)\right)dx. \quad (47)$$

By substituting (41) and (46) into (47) and applying the binomial theorem, it leads to

$$\begin{aligned}\mathbb{E}\left[\mu_{k_{c,\max}}\right] &= \int_0^{\infty}\left(1-\left(1-e^{-Lx}\sum_{k=0}^{M-1}\frac{L^k x^k}{k!}\right)^L\right)dx \\ &= \int_0^{\infty}\left(\sum_{l=1}^{L}\binom{L}{l}(-1)^{l+1}e^{-lLx}\left(\sum_{k=0}^{M-1}\frac{L^k x^k}{k!}\right)^l\right)dx \\ &= \sum_{l=1}^{L}\binom{L}{l}(-1)^{l+1}\sum_{k=0}^{(M-1)l}b_k\left(M,L,l\right)\int_0^{\infty}e^{-lLx}x^k dx.\end{aligned} \quad (48)$$

By change of variables, the integral in (48) can be further rewritten as

$$\begin{aligned}\int_0^{\infty}e^{-lLx}x^k dx &= \left(\frac{1}{lL}\right)^{k+1}\int_0^{\infty}t^k e^{-t}dt \\ &= \left(\frac{1}{lL}\right)^{k+1}\Gamma\left(k+1\right).\end{aligned} \quad (49)$$

Hence, we can get

$$\mathbb{E}\left[\mu_{k_{c,\max}}\right] = \sum_{l=1}^{L}\binom{L}{l}(-1)^{l+1} \times\sum_{k=0}^{(M-1)l}b_k\left(M,L,l\right)\left(\frac{1}{lL}\right)^{k+1}\Gamma\left(k+1\right). \quad (50)$$

From Lemma 1 and (50), the proof is completed. ■

$$\begin{aligned}\Pr\left(\mu_{k_{c,\max}} \le x\right) &= \frac{1}{(2\pi)^{L-1}}\int_{-\infty}^{\infty}\cdots\int_{-\infty}^{\infty}\prod_{l=1}^{L-1}\left(\left(\frac{L}{L-j\omega_l}\right)^M\cdot\frac{1-e^{-j\omega_l x}}{j\omega_l}\right) \\ &\quad\cdot\left(\frac{1}{2\pi}\int_{-\infty}^{\infty}\left(\frac{L}{L-j\omega_0}\right)^M\cdot\frac{1-e^{-j\omega_0 x}}{j\omega_0}d\omega_0\right)d\omega_1\cdots d\omega_{L-1} \\ &= \left(\frac{1}{(M-1)!}\cdot\gamma\left(M,Lx\right)\right)^L,\end{aligned} \quad (41)$$

$$\mathbb{E}\left[E_{c,G}\right] \ge N_g L\left(\sum_{l=1}^{L}\binom{L}{l}(-1)^{l+1}\sum_{k=0}^{(M-1)l}b_k\left(M,L,l\right)\left(\frac{1}{lL}\right)^{k+1}k!\right)+\frac{\sigma_z^2}{P_v}, \quad (42)$$

This theorem gives two immediate remarks for the operation of the proposed PW systems in two special cases: 1) multi-antenna PW systems in flat fading channels ($L = 1$) and 2) single-antenna PW systems in frequency selective fading channels ($M = 1$), which provides an important insight into understanding the influence of the numbers of multipaths and transmit antennas on the power transfer performance.

Remark 1: For $L = 1$, the average energy delivery efficiency gain is exactly given by $\mathbb{E}\left[E_{c,G}\right] = N_g M + \frac{\sigma_z^2}{P_v}$, since $b_k\left(M, 1, 1\right) = \frac{1}{k!}$, for $k = 0, \ldots, M-1$. It is observed that the efficiency is proportional to the waveform length and the number of antennas, as long as P_v is sufficiently larger then the noise power σ_z^2. Note that the gain N_g mainly comes from the PW which enables the accumulation of the power of the reference signal. A larger wavelength may require more emitted signal power after waveforming.

Remark 2: For $M = 1$, the average energy delivery efficiency gain is lower bounded by $\mathbb{E}[E_{c,G}] \geq N_g \sum_{l=1}^{L} \binom{L}{l} (-1)^{l+1} \frac{1}{l} + \frac{\sigma_z^2}{P_v}$, since $b_0(1, L, l) = 1$, for $l = 1, \ldots, L$. Actually, the summation term over the index l is equal to $\sum_{l=1}^{L} \frac{1}{l}$ [27], and we have $\mathbb{E}[E_{c,G}] \geq N_g \sum_{l=1}^{L} \frac{1}{l} + \frac{\sigma_z^2}{P_v}$, which concludes that the efficiency is increased as the number of multipaths increases. In other words, one can possibly increase the system bandwidth to improve the efficiency by digitally resolving the naturally existing multipaths in wireless environments as many as possible.

V. Simulation Results and Discussions

Computer simulations are conducted to demonstrate the performance of the proposed multi-antenna PW systems and to substantiate the analytical findings on the average energy delivery efficiency gain and the outage performance of average harvested energy. We set $P_v = 1$ and normalize the large-scale path loss because our foucs is on the WPT performance gain achieved by the multi-antenna PW technology. In addition to a UPD channel profile, i.e., setting $\rho_{m,l} = \frac{1}{L}$ in (1), a Saleh-Valenzuela (SV) channel model in IEEE 802.15.4a UWB communication standard is adopted in the simulation [32]. This channel model is typically considered in wideband applications over a central frequency ranging between 2 GHz and 6 GHz. The system bandwidth is set as 125 MHz, i.e., the sampling period $T_S = 8$ ns, and the number of resolvable multipaths is around several dozens with respect to the considered channel bandwidth.[‡‡] Notice that a larger bandwidth is configured for the multi-antenna PW system to digitally resolve the naturally existing multipaths during the channel probing phase, and the estimated CIR is then utilized for the calculation of waveforms and reference signals during the power transfer phase. Otherwise, the estimated CIR is likely to be a single tap in spite of abundant multipaths in wireless environments. We ingore the noise power by setting $\sigma_z^2 = 0$, since the required signal power for wirelessly charging (at least -10 dBm) is much higher than the common noise power level (-93 dBm at 125 MHz bandwidth). The default values in the stopping criterion of the proposed algorithm in Table I are set as $\varepsilon = 10^{-3}$ or $I_{\max} = 3$. In addition, the WPT performance of the conventional narrow-band beamforming scheme is included for performance comparison. For this scheme, the total bandwidth B is partitioned into 30 subbands, and the strongest subband is selected to perform the conventional narrow-band beamforming as in [18], which is called frequency-domain approach in this paper.

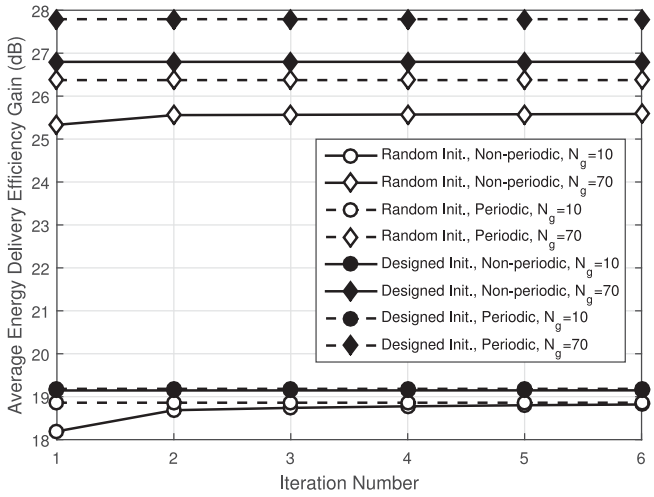

Fig. 3. Average energy delivery efficiency gain of the proposed algorithm with the random and designed initialization for various iteration numbers in the UWB SV channels ($M = 4$ and $N_v = 100$).

Fig. 3 shows the average energy delivery efficiency gain of the proposed algorithm in Table I with the random and designed initialization for various iteration numbers in the UWB SV channels. The number of transmit antennas and the length of reference signals are given by $M = 4$ and $N_v = 100$, respectively. For the random initialization, the reference signal is initialized with complex binary signals, i.e., $v[n] \in \{\pm\frac{1}{\sqrt{2}} \pm j\frac{1}{\sqrt{2}}\}$. We can make two observations from this figure. First, for a given initialization scheme and a fixed waveform length, the multi-antenna PW system with the periodic transmission of reference signals can achieve better converged performance than that with the non-periodic transmission because the former allows for fully concentrating the power on the best selected frequency, whereas the later causes the power leakage to other neighboring frequencies. Second, the proposed system with the designed initialization outperforms that with the random initialization, and its performance can quickly get converged within two iterations. Hence, the designed initialization scheme is utilized throughout the following simulation.

Fig. 4 and Fig. 5 show the average energy delivery efficiency gain with the non-periodic and periodic transmissions of reference signals, respectively, for different lengths of waveforms and reference signals in the UWB SV channels. The number of transmit antennas is given by $M = 4$. For the case of non-periodic transmission, it is found that the average energy delivery efficiency gain can be dramatically improved by

[‡‡]The system could be possibly operated on a selective portion of the industrial, scientific and medical radio band (ISM band) band on which the proposed waveform concentrates its power, and the remaining bandwidth is reserved for wireless information transmission.

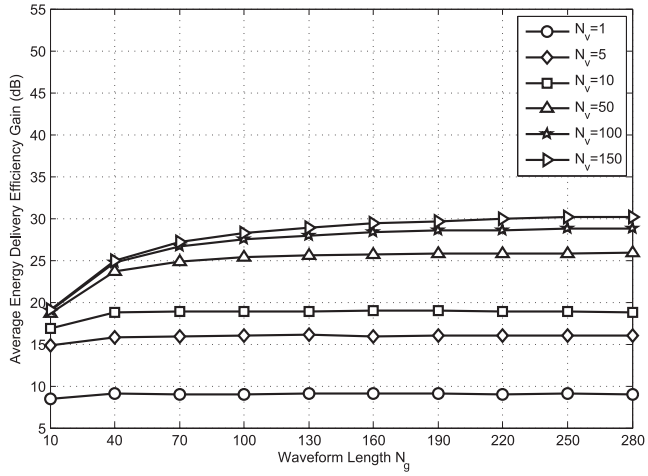

Fig. 4. Average energy delivery efficiency gain of the proposed algorithm with the non-periodic transmission of reference signals for different lengths of waveforms and reference signals in the UWB SV channels ($M = 4$).

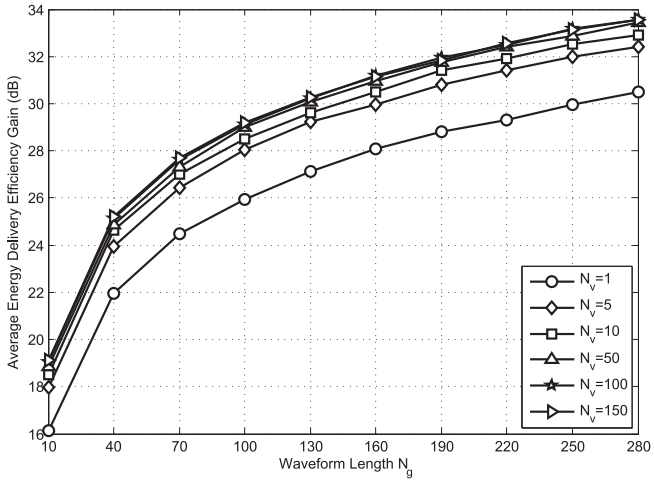

Fig. 5. Average energy delivery efficiency gain of the proposed algorithm with the periodic transmission of reference signals for different lengths of waveforms and reference signals in the UWB SV channels ($M = 4$).

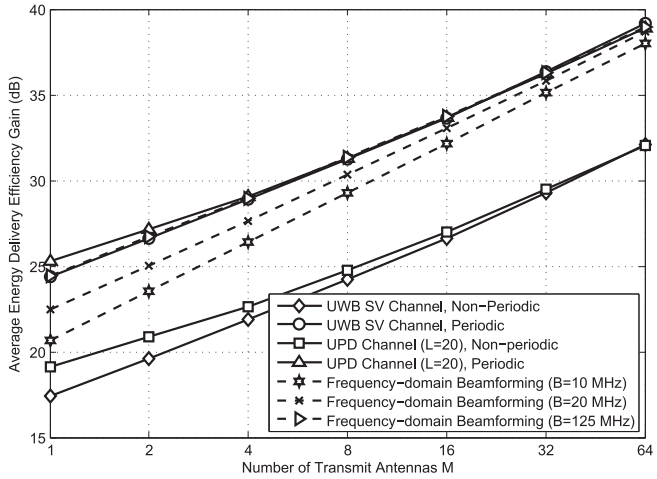

Fig. 6. Comparisons of average energy delivery efficiency gains between the multi-antenna PW system and the frequency-domain beamforming system for various numbers of transmit antennas in the UWB SV and the UPD channels ($N_g = N_v = 100$).

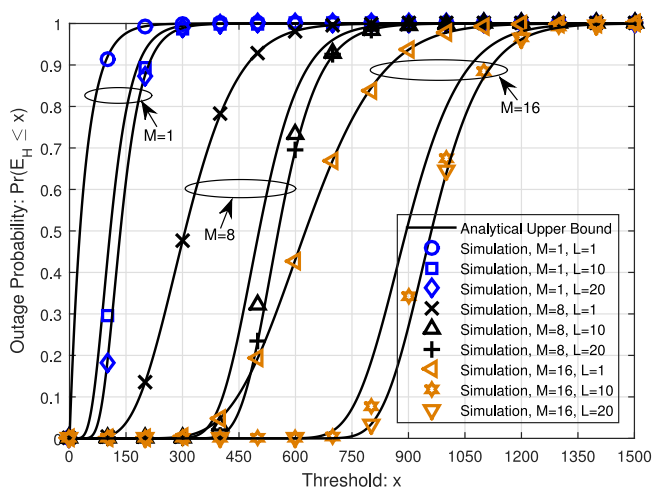

Fig. 7. Outage performance of the average harvested energy and the analytical upper bound for the multi-antenna PW systems with the periodic transmission of reference signals under the UPD channel profile ($N_v = 20$ and $N_g = 40$).

increasing the lengths of waveforms or reference signals. Taking an example of $N_g = 280$, the performance improvement is as large as 22 dB when N_v is increased from 1 to 150. We can also see that the performance improvement becomes moderate as the values of N_v and N_g increase. Similar performance trends can be observed for the case of periodic transmission in Fig. 5. For $N_v = 150$ and $N_g = 280$, the average energy delivery efficiency gain of the proposed multi-antenna PW system is around 34 dB. It is demonstrated from these two figures that for given values of N_v and N_g, the performance of the multi-antenna PW system with the periodic transmission of reference signals is much superior to that with the non-periodic transmission.

Fig. 6 compares the performances of the multi-antenna PW system and the frequency-domain beamforming system, in terms of the average energy delivery efficiency gain. The lengths of the waveforms and the reference signals are given by $N_g = N_v = 100$, and the number of multipaths in the UPD channel profile is set as $L = 20$. The frequency-domain beamforming approach is simulated in the UWB SV channel, and its emitted signal power is set the same as the proposed scheme for a fair comparison. It exhibits that the energy delivery efficiency gain of the multi-antenna PW system with the periodic transmission of reference signals is 5 dB better than that with the non-periodic transmission for various numbers of transmit antennas. Furthermore, one can see that when B is increased from 10 MHz to 125 MHz, the performance gap between the frequency-domain approach and our proposed time-domain approach with the periodic transmissions of reference signals becomes narrow in the UWB SV channel, since they both utilize the diversity gains of the wireless channels.

Fig. 7 shows the exact outage probability of the average harvested energy and the derived upper bound given in (38) under the UPD channel profile for various numbers of transmit antennas and multipaths. The lengths of periodic reference signals and waveforms are set as $N_v = 20$ and $N_g = 40$, respectively. Obviously, the outage performance gets better when the

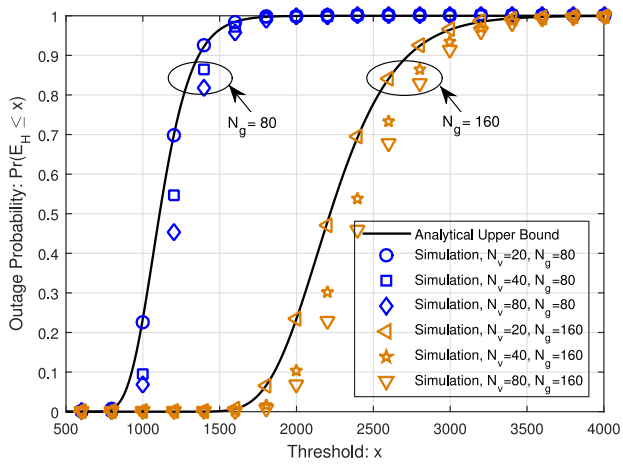

Fig. 8. Outage performance of the average harvested energy and the analytical upper bound for different lengths of waveforms and reference signals under the UPD channel profile ($M = 8$ and $L = 20$).

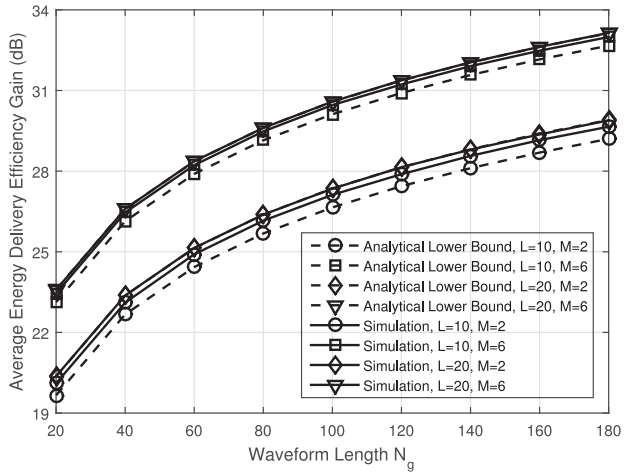

Fig. 9. Average energy delivery efficiency gain and the analytical lower bound for the multi-antenna PW systems with the periodic transmission of reference signals under the UPD channel profile ($N_v = 20$).

numbers of transmit antennas and multipaths increase owing to the higher frequency-selective and antenna gains on the combined channel frequency responses. As expected, the analytical results are in close agreement with the simulation results when $N_v = L = 20$ or $L = 1$, thereby validating the correctness of the proposed analytical expressions in Theorem 3. In addition, it is clearly observed that the upper bounds are quite tight for the cases with $L = 10$. In order to verify the tightness of the derived upper bound under different lengths of waveforms and reference signals, the simulation results and analytical results for the outage performance are compared in Fig. 8, where we set $M = 8$ and $L = 20$ for the UPD channel profile. We can find that the outage probability decreases as the values of N_v and N_g increase. Again the analytical results for the upper bounds are very close to the simulated ones when $N_v = L = 20$. As the value of N_v increases, the difference between the two performance results slightly increases.

Fig. 9 depicts the average energy delivery efficiency gain as a function of the waveform length and the derived lower bound given in (42) under the UPD channel profile for various numbers of transmit antennas and multipaths. The length of reference signals is given by $N_v = 20$. Our results reveal that a substantial improvement can be achieved by increasing the waveform length, the number of transmit antennas, and the resolvable number of multipaths. It is evident from this figure that the simulation results and the analytical results fit perfectly when $N_v = L = 20$, which confirms our theoretical findings in Theorem 4. The proposed lower bound is also very tight in the cases with $L = 10$, and therefore, it can serve as a good lower bound for predicting the performance of the proposed multi-antenna PW system in multipath environments.

VI. Conclusion

In this paper, we investigated a joint power waveforming and beamfoming design for WPT, in which the waveforms on multiple transmit antennas driven by a common reference signal are optimized to maximize the gain of energy delivery efficiency. We proved that under the periodic transmission of a reference signal, the optimal waveforms exhibit single-tone structures with appropriate tone selection and power allocation over transmit antennas. It was analytically demonstrated that the corresponding optimal reference signal can be simply determined by picking a frequency component with the largest sum-power of channel frequency responses over transmit antennas. Analytic upper and lower bound expressions for the outage performance of the average harvested energy and the energy delivery efficiency gain were derived in closed forms under the UPD channel profile. The analytic results allowed us to quantify the influence of several system parameters, e.g., the number of transmit antennas, the channel length, the waveform length, on the WPT performance. Simulation results revealed that a 20–30dB improvement can be achieved by employing the proposed scheme compared to the conventional narrow-band beamforming scheme.

References

[1] J. Jin, J. Gubbi, S. Marusic, and M. Palaniswami, "An information framework for creating a smart city through Internet of Things," *IEEE Internet Things J.*, vol. 1, no. 2, pp. 112–121, Apr. 2014.

[2] A. Luigi, I. Antonio, and M. Giacomo, "The Internet of Things: A survey," *Comput. Netw.*, vol. 54, no. 15, pp. 2787–2805, Oct. 2010.

[3] P. Kamalinejad, C. Mahapatra, Z. Sheng, S. Mirabbasi, V. C. M. Leung, and Y. L. Guan, "Wireless energy harvesting for the Internet of Things," *IEEE Commun. Mag.*, vol. 53, no. 6, pp. 102–108, Jun. 2015.

[4] S. Sudevalayam and P. Kulkarni, "Energy harvesting sensor nodes: Survey and implications," *IEEE Commun. Surveys Tuts.*, vol. 13, no. 3, pp. 443–461, Jul.–Sep. 2011.

[5] X. Lu, P. Wang, D. Niyato, D. I. Kim, and Z. Han, "Wireless charging technologies: Fundamentals, standards, and network applications," *IEEE Commun. Surveys Tuts.*, vol. 18, no. 2, pp. 1413–1452, Apr.–Jun. 2016.

[6] N. B. Carvalho *et al.*, "Wireless power transmission: R&D activities within Europe," *IEEE Trans. Microw. Theory Techn.*, vol. 62, no. 4, pp. 1031–1045, Apr. 2014.

[7] M.-L. Ku, W. Li, Y. Chen, and K. J. Ray Liu, "Advances in energy harvesting communications: Past, present, and future challenges," *IEEE Commun. Surveys Tuts.*, vol. 18, no. 2, pp. 1384–1412, Apr.–Jun. 2016.

[8] S. Kim *et al.*, "Ambient RF energy-harvesting technologies for self-sustainable standalone wireless sensor platforms," *Proc. IEEE*, vol. 102, no. 11, pp. 1649–1666, Nov. 2014.

[9] X. Chen, Z. Zhang, H.-H. Chen, and H. Zhang, "Enhancing wireless information and power transfer by exploiting multi-antenna techniques," *IEEE Commun. Mag.*, vol. 53, no. 4, pp. 133–141, Apr. 2015.
[10] K. Huang and V. K. N. Lau, "Enabling wireless power transfer in cellular networks: Architecture, modeling and deployment," *IEEE Trans. Wireless Commun.*, vol. 13, no. 2, pp. 902–912, Feb. 2014.
[11] G. Yang, C. K. Ho, and Y. L. Guan, "Multi-antenna wireless energy transfer for backscatter communication systems," *IEEE J. Sel. Areas Commun.*, vol. 33, no. 12, pp. 2974–2987, Dec. 2015.
[12] Z. Wang, L. Duan, and R. Zhang, "Adaptively directional wireless power transfer for large-scale sensor networks," *IEEE J. Sel. Areas Commun.*, vol. 34, no. 5, pp. 1785–1800, May 2016.
[13] X. Chen, X. Wang, and X. Chen, "Energy-efficient optimization for wireless information and power transfer in large-scale MIMO systems employing energy beamforming," *IEEE Wireless Commun. Lett.*, vol. 2, no. 6, pp. 667–670, Dec. 2013.
[14] G. Yang, C. K. Ho, R. Zhang, and Y. L. Guan, "Throughput optimization for massive MIMO systems powered by wireless energy transfer," *IEEE J. Sel. Areas Commun.*, vol. 33, no. 8, pp. 1640–1650, Aug. 2015.
[15] S. Kashyap, E. Bjornson, and E. G. Larsson, "On the feasibility of wireless energy transfer using massive antenna arrays," *IEEE Trans. Wireless Commun.*, vol. 15, no. 5, pp. 3466–3480, May 2016.
[16] L. Liu, R. Zhang, and K.-C. Chua, "Multi-antenna wireless powered communication with energy beamforming," *IEEE Trans. Commun.*, vol. 62, no. 12, pp. 4349–4361, Dec. 2014.
[17] X. Wu, W. Xu, X. Dong, H. Zhang, and X. You, "Asymptotically optimal power allocation for massive MIMO wireless powered communications," *IEEE Wireless Commun. Lett.*, vol. 5, no. 1, pp. 100–103, Feb. 2016.
[18] Y. Zeng and R. Zhang, "Optimized training for net energy maximization in multi-antenna wireless energy transfer over frequency-selective channel," *IEEE Trans. Commun.*, vol. 63, no. 6, pp. 2360–2373, Jun. 2015.
[19] B. Clerckx and E. Bayguzina, "Waveform design for wireless power transfer," *IEEE Trans. Signal Process.*, vol. 64, no. 23, pp. 5972–5975, Dec. 2016.
[20] Y. Zeng, B. Clerckx, and R. Zhang, "Communications and signals design for wireless power transmission," *IEEE Trans. Commun.*, vol. 65, no. 5, pp. 2264–2290, May 2017.
[21] K. Huang and E. Larsson, "Simultaneous information and power transfer for broadband wireless systems," *IEEE Trans. Signal Process.*, vol. 61, no. 23, pp. 5972–5986, Dec. 2013.
[22] S. Lee and R. Zhang, "Distributed wireless power transfer with energy feedback," *IEEE Trans. Signal Process.*, vol. 65, no. 7, pp. 1685–1699, Apr. 2017.
[23] Y. Zeng and R. Zhang, "Optimized training design for wireless energy transfer," *IEEE Trans. Commun.*, vol. 63, no. 2, pp. 536–550, Feb. 2015.
[24] G. Yang, C. K. Ho, and Y. L. Guan, "Dynamic resource allocation for multiple-antenna wireless power transfer," *IEEE Trans. Signal Process.*, vol. 62, no. 14, pp. 3565–3577, Jul. 2014.
[25] J. Xu and R. Zhang, "A general design framework for MIMO wireless energy transfer with limited feedback," *IEEE Trans. Signal Process.*, vol. 64, no. 10, pp. 2475–2488, May 2016.
[26] J. Xu and R. Zhang, "Energy beamforming with one-bit feedback," *IEEE Trans. Signal Process.*, vol. 62, no. 20, pp. 5370–5381, Oct. 2014.
[27] M.-L. Ku, Y. Han, H.-Q. Lai, Y. Chen, and K. J. Ray Liu, "Power waveforming: Wireless power transfer beyond time-reversal," *IEEE Trans. Signal Process.*, vol. 64, no. 22, pp. 5819–5834, Nov. 2016.
[28] X. Zhou, C. K. Ho, and R. Zhang, "Wireless power meets energy harvesting: A joint energy allocation approach in OFDM-based system," *IEEE Trans. Wireless Commun.*, vol. 15, no. 5, pp. 3481–3491, May 2016.
[29] B. Wang, Y. Wu, F. Han, Y.-H. Yang, and K. J. Ray Liu, "Green wireless communications: A time-reversal paradigm," *IEEE J. Sel. Areas Commun.*, vol. 29, no. 8, pp. 1698–1710, Sep. 2011.
[30] S. Budišin, "Golay complementary sequences are superior to PN sequences," in *Proc. IEEE Int. Conf. Syst. Eng.*, 1992, pp. 101–104.
[31] Y. Han, Y. Chen, B. Wang, and K. J. Ray Liu, "Time-reversal massive multipath effect: A single-antenna 'massive MIMO' solution," *IEEE Trans. Commun.*, vol. 64, no. 8, pp. 3382–3394, Aug. 2016.
[32] A. A. M. Saleh and R. A. Valenzuela, "A statistical model for indoor multipath propagation," *IEEE J. Sel. Areas Commun.*, vol. SAC-5, no. 2, pp. 128–137, Feb. 1987.
[33] Q. T. Zhang and H. G. Lu, "A general analytical approach to multi-branch selection combining over various spatially correlated fading channels," *IEEE Trans. Commun.*, vol. 50, no. 7, pp. 1066–1073, Jul. 2002.
[34] I. S. Gradshteyn and I. M. Ryzhik, *Tables of Integrals, Series and Products*. New York, NY, USA: Academic, 2007.

Meng-Lin Ku (M'11) received the B.S., M.S., and Ph.D. degrees from the National Chiao Tung University, Hsinchu, Taiwan, in 2002, 2003, and 2009, respectively, all in communication engineering. From 2009 to 2010, he was a Postdoctoral Research Fellow with Prof. L.-C. Wang in the Department of Electrical and Computer Engineering, National Chiao Tung University and with Prof. V. Tarokh in the School of Engineering and Applied Sciences, Harvard University. In August 2010, he became a Faculty Member in the Department of Communication Engineering, National Central University, Taoyuan City, Taiwan, where he is currently an Associate Professor. During the summer of 2013, he was a Visiting Scholar in the Signals and Information Group of Prof. K. J. Ray Liu at the University of Maryland. His research interests include green communications, cognitive radios, and optimization of radio access. He received the Best Counseling Award in 2012 and the university-level Best Teaching Award in 2014, 2015, and 2016 at the National Central University. He also received the Exploration Research Award of the Pan Wen Yuan Foundation, Taiwan, in 2013.

Yi Han received the B.S. degree in electrical engineering (with highest Hons.) from Zhejiang University, Hangzhou, China, in 2011, and the Ph.D. degree from the Department of Electrical and Computer Engineering, University of Maryland, College Park, MD, USA, in 2016. He is currently the Wireless Architect in the Origin Wireless, Inc., Greenbelt, MD, USA. His research interests include wireless communication and signal processing.

He received the Class A Scholarship from Chu Kochen Honors College, Zhejiang University, in 2008, and the Best Student Paper Award of IEEE International Conference on Acoustics, Speech and Signal Processing in 2016.

Beibei Wang (SM'15) received the B.S. degree (highest Hons.) from the University of Science and Technology of China, Hefei, China, in 2004, and the Ph.D. degree from the University of Maryland, College Park, MD, USA, in 2009, both in electrical engineering. She was at the University of Maryland as a Research Associate from 2009 to 2010, and with Qualcomm Research and Development from 2010 to 2014. Since 2015, she has been with the Origin Wireless, Inc., Greenbelt, MD, USA, where she is currently the Chief Scientist, Wireless. She is a coauthor of *Cognitive Radio Networking and Security: A Game-Theoretic View* (Cambridge University Press, 2010). Her research interests include wireless communications and signal processing. She received the Graduate School Fellowship, the Future Faculty Fellowship, the Dean's Doctoral Research Award from the University of Maryland, and the Overview Paper Award from the IEEE Signal Processing Society in 2015.

K. J. Ray Liu (F'03) was named, in 2007, a Distinguished Scholar-Teacher of University of Maryland, College Park, MD, USA, where he is currently the Christine Kim Eminent Professor of Information Technology. He leads the Maryland Signals and Information Group conducting research encompassing broad areas of information and communications technology with recent focus on smart radios for smart life.

He received the 2016 IEEE Leon K. Kirchmayer Technical Field Award on graduate teaching and mentoring, IEEE Signal Processing Society 2014 Society Award, and IEEE Signal Processing Society 2009 Technical Achievement Award. Recognized by Thomson Reuters as a Highly Cited Researcher, he is a Fellow of AAAS. He is a member of IEEE Board of Director as Division IX Director. He was the President of IEEE Signal Processing Society, where he served as the Vice President—Publications and Board of Governor. He was the Editor-in-Chief of the IEEE SIGNAL PROCESSING MAGAZINE. He also received teaching and research recognitions from the University of Maryland including university-level Invention of the Year Award; and college-level Poole and Kent Senior Faculty Teaching Award, Outstanding Faculty Research Award, and Outstanding Faculty Service Award, all from A. James Clark School of Engineering.